Novel Hybrid Feedforward Wavelet Clipping – ANFIS for Hydrogen Supply in Open Cathode PEM Fuel Cell

Triyanto Pangaribowo*,***‡, Wahyu Mulyo Utomo**, Deni Shidqi Khaerudini***, Afarulrazi Abu Bakar**

* Department of Electrical Engineering, Faculty of Engineering, Universitas Mercu Buana, Jakarta Indonesia

** Faculty of Electrical and Electronic Engineering, University Tun Hussein Onn Malaysia, Johor, Malaysia

*** Research Center for Advanced Materials, National Research and Innovation Agency (BRIN), Bld. 440 Kawasan Puspiptek Serpong, South Tangerang, 15314 Banten, Indonesia

(triyanto.pangaribowo@mercubuana.ac.id, wahyu@uthm.edu.my, deni.shidqi.khaerudini@brin.go.id, afarul@uthm.edu.my)

‡ Corresponding Author; Triyanto Pangaribowo, Universitas Mercu Buana, Jakarta, Indonesia, triyanto.pangaribowo@mercubuana.ac.id

Received: 27.12.2023 Accepted:31.01.2024

Abstract- The open cathode PEM Fuel Cell is a generator that relies on an electrochemical reaction between oxygen and hydrogen to produce electricity. In open-cathode fuel cells, oxygen is drawn from the air using fans, while hydrogen gas needs to be supplied through a pressure tube. Hydrogen gas significantly contributes to maintaining the generator's performance. Raising the load on fuel cell generators escalates hydrogen consumption. This poses an issue when the hydrogen supply doesn't swiftly adapt to load changes, leading to fluctuations in generator output. These fluctuations generate noise characterized by the dissonance between frequency and amplitude, gradually oscillating. Additionally, it mentions that filtering techniques, while used to reduce noise, might inadvertently increase the amplitude. Present studies indicate the effectiveness of ANFIS control for various applications. However, its sensitivity to noise affects its accuracy performance, rendering it suboptimal. Hence, this study introduces a hybrid control system to ensure stable hydrogen gas flow, employing the feedforward wavelet clipping method combined with ANFIS. The clipping technique restricts large amplitudes, while wavelets filter high noise. This system is implemented on an experimentally validated fuel cell model. The performance analysis of the control system demonstrates that the proposed method achieves high accuracy and swiftly recovers in the event of a disturbance.

Keywords Open cathode PEM fuel cell, control, wavelet, clipping, ANFIS.

1. Introduction

Currently, open cathode PEM fuel cells are an environmentally friendly energy device option[1], offering advantages such as low parasitic losses [2] and a simpler structure[3]. In this open cathode fuel cell, oxygen is taken from the air using fans to reduce the cost of providing pure oxygen[4]. Fans are utilized to regulate temperature and supply oxygen gas to the fuel cell[5]. Meanwhile, hydrogen gas has high economic value due to the high costs of the purification process, so its use must be controlled[6][7]. Controlling the flow of hydrogen is crucial not only to save hydrogen fuel consumption[7] but also to maintain fuel cell performance[8][9]. Hydrogen gas starvation can lead to a drop in power, consequently disrupting the supply of electricity to the load[10]. Power drops can occur due to load fluctuations[11]. Output power instability is caused by rapid load changes[12]. This could potentially lead to an output signal that is also prone to containing noise[13]. When a fuel cell operates under varying loads, it can produce fluctuations in current and voltage. These variations might lead to changes in the electrochemical processes within the cell[14], causing fluctuations in the output signal. Therefore, a reliable hydrogen gas flow control system is essential to effectively address these disturbances[15].

Numerous strategies for regulating hydrogen flow rates in fuel cells have been proposed, including microcontroller-

based automatic methods[16], Fuzzy Sliding Mode Controller[17], PID controller[18], Fuzzy logic control systems ensuring stability of output power during load variations[9][19][20][21], a combination of fuzzy logic and PID for maintaining fuel cell output voltage stability[22], robust adaptive neural network control[23], fuzzy self-adaptive PID controller[24], problem-solving using TRIZ to determine optimal gas flow control parameters [25], and the Fractional Order PID Controller method[26].

However, both PID (Proportional-Integral-Derivative) and fuzzy control systems exhibit limitations when implemented in open-cathode PEM fuel cell applications, particularly in scenarios where the system is non-linear and displays high dynamics, demanding precision[27]. In systems characterized by elevated dynamics, PID control encounters challenges in parameter tuning, leading to a reduction in accuracy[28][29]. The limitations of fuzzy control systems stem from the lack of guaranteed stability, the reliance on trial and error for optimization, and the difficulty in tuning multiple parameters (defuzzification, inference, and fuzzification) in systems that undergo rapid changes over time[30]. However, fuzzy logic controllers exhibit the capability to effectively manage systems without necessitating extensive mathematical analysis[31][32]. The integration of fuzzy PID methods yields superior results in comparison to using PID or Fuzzy independently[33][34].

Hence, a robust control system is essential to manage fluctuations in the open cathode PEM fuel cell. A robust hydrogen flow control system can stabilize the output voltage because delay in the hydrogen gas supply can influence the power output of the fuel cell[14]. The cause is a discrepancy between changing load demands and insufficient gas supply[35]. To ensure a consistent hydrogen supply, feedforward control systems are required for constant and variable loads[36][37]. Utilizing wavelets for noise reduction is an effective strategy to increase accuracy because there are low-pass and high-pass filters[38]. ANFIS control demonstrates high accuracy[39], particularly when supported by both quality and quantity of input data[40][41]. The efficacy of the ANFIS method is also contingent upon well-chosen parameters associated with the membership function[42].

Therefore in this paper introduces a novel application of a feedforward wavelet clipping-ANFIS (FWC-ANFIS) controller specifically designed for optimizing hydrogen flow in open cathode PEM fuel cell. The control system aims to regulate the hydrogen flow rate. The main contribution of this paper lies in the application of a new control system method to optimize hydrogen supply in open cathode PEM fuel cell during fluctuations. The paper is organized into several sections, starting with an introduction followed by research methods section encompassing the experimental setup, mathematical model of fuel cell, and the FWC-ANFIS. Subsequently, the simulation results and discussion section critically examines the findings. Finally, the findings are summarized in the conclusion section.

2. Research Methodology

This section discusses several stages, beginning with the experimental setup, followed by the mathematical fuel cell model, and concluding with the FWC - ANFIS control model.

2.1. Experimental Configuration

The aim of this experiment is to obtain real data from an open cathode fuel cell. It is important to know the actual characteristics of fuel cells to be used in designing accurate fuel cell models. The utilized cell specifications include an active area measuring 5.5 cm x 29 cm, a cell size of 34 cm x 7 cm, and a thickness of 4 mm. Fig 1. shows a detailed schematic diagram of a fuel cell experiment.

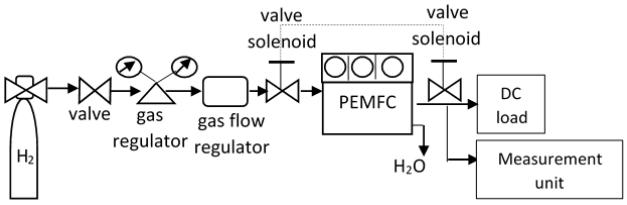

Fig. 1. Schematic diagram of a open cathode PEM fuel cell experiment.

The devices used in this experiment comprise a 73-cell open-cathode PEM fuel cell with a maximum power of 3kW, a gas pressure regulator, instruments for measuring power, current, and voltage, a DC load regulator to manage load fluctuations, an Arduino-controlled control valve, and a PC for monitoring.

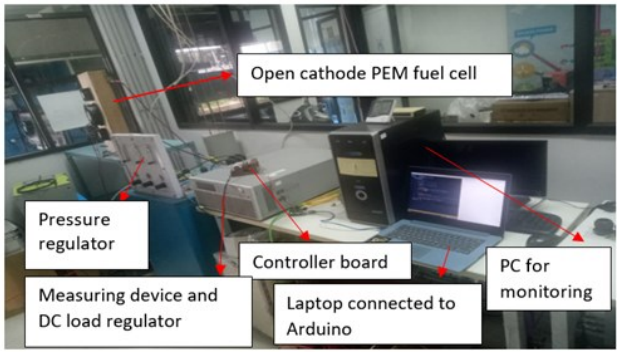

Fig. 2. Experimental configuration for collecting data from open cathode PEM fuel cells.

The experimental stage begins with a 30-minute warm-up period for the fuel cell, operating without a load. The hydrogen gas flow in this study was regulated using a regulator set between 1 L/min up to 10 L/min. Meanwhile, oxygen gas is taken from the air using a 48V DC fan. The measured variables in this experiment include hydrogen gas flow, voltage, current, and fuel cell output power.

2.2. Mathematical Model of Fuel Cell

Mathematical modeling of fuel cell systems efficiently allows for an in-depth analysis of various performance influencing parameters, such as hydrogen gas flow[43]. Fuel cells generally produce output in the form of DC voltage[44]. The output voltage of a fuel cell stack (V_{FC}) is determined by

multiplying the single cell voltage by the corresponding number of cells (Ncell) in the stack[45][46].

$$V_{FC} = N_{cell}(E_{Nernst} - V_{Act} - V_{Ohmic} - V_{con}) \quad (1)$$

The ideal output voltage of a fuel cell (E_{Nernst}) is affected by several losses: activation drop voltage (V_{Act}), resistance related voltage drop during proton movement (VOhmic), and concentration-related voltage drop due to changes in concentration (V_{Con})[47]. Equation (2) is utilized for calculating E_{Nernst}.

$$E_{Nernst} = 1.229 - 0.00085(T - 298.15) + 0.000043 (\ln(P_{h_2}) + 0.5 \ln(P_{o_2}) \quad (2)$$

Voltage drop caused by activation losses can be estimated using the Tafel equation;

$$V_{act} = -\left(\frac{R*T}{2*\alpha*F}\right) * \log\left(\frac{i_L}{i_0}\right) \quad (3)$$

At an operating temperature (T) of 333 K, with a transfer coefficient (α) of 0.5, Faraday's constant (F) of 96487 C/mol, an ideal gas constant (R) of 8.314 J/mol K, a limiting current density (iL) of 1.4 A/cm2, and an exchange current density (i0) of 10^-6.912 A/cm2. The ohmic losses (V_{ohmic}) are estimated using Ohm's law:

$$V_{ohmic} = -(i * r) \quad (4)$$

Where r is internal resistance is 0.19 Ohm-cm^2. The mass transport can be calculated using the following equation:

$$V_{con} = -\alpha * i^k * \ln\left(1 - \frac{i}{i_l}\right) \quad (5)$$

In mass transport, the constant (k) with a value of 1.1 is utilized. Refer to reference[19][48], Hydrogen vale molar constant (KH_2) is 0.843 mol/s.atm and for Oxygen valve constant (KO_2) is 2.52 mol/s.atm.

$$K_{H_2} = \frac{qH_2}{PH_2} = \frac{k_{a\,n}}{\sqrt{MH_2}} \quad (6)$$

The molar flow of hydrogen is represented by the symbol qH_2, whereas PH_2 denotes the partial pressure of hydrogen. In addition, MH_2 stands for the molar mass of hydrogen, and Kan represents the anode valve constant. Equation (7) can be used to compute the reacting hydrogen flow, which is represented by the symbol $q^r_{H_2}$.

$$q^r_{H_2} = \frac{N_{cell}.I}{2F} = 2K_r I \quad (7)$$

The modelling constant is denoted by Kr with the value of 1.4251×10-6 kmol s^{-1} A^{-1}

$$K_r = \frac{N_{cell}}{4F} \quad (8)$$

The stack current is represented by the symbol I. The mathematical equation for the partial pressure of hydrogen gas, represented by the symbol PH_2, is as follows:

$$P_{H_2} = \frac{\frac{1}{K_{H_2}}}{1 + \tau H_2 s}\left(q^{in}_{H_2} - 2K_r I\right) \quad (9)$$

The symbol $q^{in}_{H_2}$ represents the flow rate of hydrogen input, while the symbol $\tau H_2 s$ represents the hydrogen time constant. To calculate τ_{H_2} use the following equation:

$$\tau_{H_2} = \frac{V_{an}}{K_{H_2} RT} \quad (10)$$

The partial pressure of oxygen gas at the fuel cell cathode can be calculated by the equation (11).

$$P_{O_2} = \frac{{}^1/_{K_{O_2}}}{1+\tau_{O_2}}\left(q^{in}_{O_2} - K_r I\right) \quad (11)$$

The molar flow of hydrogen gas can be determined by equation[49].

$$q_{H_2} = \frac{N_0 I_{stack}}{2FU} \quad (12)$$

Static and dynamic models were built using Matlab simulink based on fuel cell mathematical equations. The model simulates PEM fuel cells by depicting the correlation between output voltage and the partial pressures of hydrogen and oxygen. The total fuel cell voltage (V_{FC}) is calculated using the following equation.

$$V_{FC} = V_{out} * N_{Cell} \quad (13)$$

Where the number of cells (N_{cell}) is 73 cells.

2.3. Control Design

The control system's design integrates wavelet clipping and ANFIS techniques for controlling hydrogen gas flow. Fig. 3 shows the H_2 flow rate controller block.

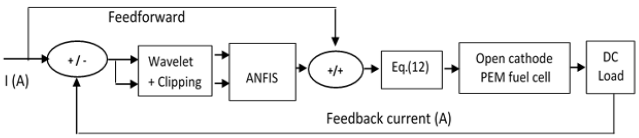

Fig. 3. Hydrogen flow rate control block.

In the control system, the stack current is utilized as the setpoint and manipulated using equation (12) to convert it into hydrogen gas flow. This hydrogen flow is then fed forward and summed with the control system output.

2.4. Wavelet Structure

The 5/3 wavelet transform is commonly used in image compression and signal processing[50][51]. The wavelet produces two outputs: approximation and detail. The basic equations for 5/3 wavelet transform (discrete version) can be expressed as equations (14) until (17). The sequence of 5/3 wavelet analysis and synthesis is presented through the following equation

Analysis filters:

$$h(z) = -\frac{1}{8}z^{-2} + \frac{1}{4}z^{-1} + \frac{3}{4} + \frac{1}{4}z^{1} - \frac{1}{8}z^{2} \quad (14)$$

$$g(z) = -\frac{1}{2}z^{-1} + 1 - \frac{1}{2}z^{1} \quad (15)$$

Synthesis filters:

$$\bar{h}(z) = \frac{1}{2}z^{-1} + 1 + \frac{1}{2}z^{1} \quad (16)$$

$$\bar{g}(z) = -\frac{1}{8}z^{-2} - \frac{1}{4}z^{-1} + \frac{3}{4} - \frac{1}{4}z^{1} - \frac{1}{8}z^{2} \quad (17)$$

These outputs are utilized as inputs for the fuzzy neural network controller. For a clearer understanding of the wavelet structure utilized in this study, please refer to Fig. 4, which corresponds to reference[51].

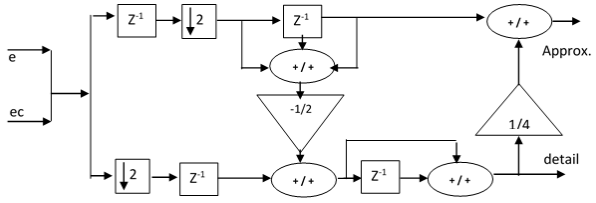

Fig. 4. Wavelet structure.

The wavelet has two inputs: error (e) and change in error (ec) derived from the hydrogen flow signal.

2.5. Clipping Technique

The clipping technique aims to diminish noise by constraining the signal's amplitude to a predefined threshold [52]. This is necessary as the application of a filter may lead to the resurgence of peak amplitudes.

Mathematically, the clipping operation clip (x,a,b) for a value x is defined as[53]:

$$clip(x,a,b) = \begin{cases} a & if\ x < a \\ x & if\ a \le x \le b \\ b & if\ x > b \end{cases} \quad (18)$$

Where:
x is the input signal.
a is the lower limit of the range.
b is the upper limit of the range

2.6. Adaptive Neuro Fuzzy Inference System

The structure of the Adaptive Neuro Fuzzy Inference System (ANFIS) typically includes 5 layers using the fuzzy Sugeno type[40][54]. The Sugeno fuzzy system is expressed in the form of the following If-then rule :

$$\text{If x is A1 and y is B1, then f1} = \text{p1x} + \text{q1y} + \text{r1}$$

$$\text{If x is A2 and y is B2, then f2} = \text{p2x} + \text{q2y} + \text{r2}$$

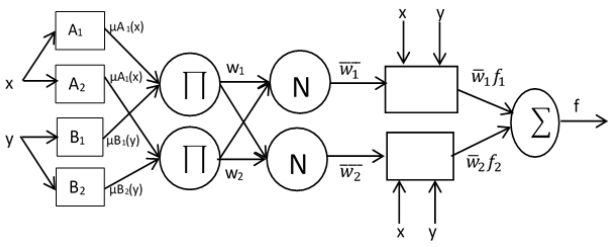

Fig. 5. ANFIS architecture.

Layer 1: This layer serves as the fuzzification layer, housing a membership function with two inputs: x and y.

$O_i^1 = \mu A_i(x)$ and $O_i^1 = \mu B_i(y)$,i =1,2 (19)

Where O_i^1 is a symbol that represents the membership function of each node label input A_i and B_i. In this particular scenario, the membership function $\mu A_i(x)$ is chosen to exhibit a bell-shaped structure, with a highest value of 1 and a lowest value of 0, as depicted in the illustration below:

$$O_i^1 = \mu A_i(x) = \frac{1}{1 + \left|(\frac{x - c_i}{a_i})^2\right|^{b_i}} \quad (20)$$

Where a_i, b_i, and c_i represent sets of parameters adjusted to the specific requirements of the bell-shaped membership function.

Layer 2: Each node in this layer is depicted as a circle with the symbol Π Every node contains the multiplication of two input signals, and its output is calculated as the product using T-norm (logical AND).

$$O_i^2 = w_i = \mu A_i(x) * \mu B_i(y), i = 1,2 \quad (21)$$

where μA_i (x) and μB_i (y) are the membership functions for the input variables x and y. The resulting value w_i represents the firing strength or degree of membership for the i-th rule. Each output node corresponds to the firing strength of a specific rule.

Layer 3: Every circle-shaped element marked with N represents a node. In this layer, a normalization process takes place, which includes performing arithmetic addition and division. To elaborate, the i-th node calculates the ratio between the firing strength of the i-th rule and the collective sum of firing strengths across all rules in the following equation:

$$O_i^3 = \overline{w_i} = \frac{w_i}{w_1 w_2}, i = 1,2 \quad (22)$$

The calculated values, referred to as w_i, are called normalized firing strengths.

Layer 4: Every square-shaped element within this layer represents a node and executes the multiplication of the normalized output from layer 3, labeled as $\overline{w_i}$ with the 'then' segment of the fuzzy rule, noted as f_i, the equation as follows:

$$O_i^4 = \overline{w_i} f_i = \overline{w_i}(p_i x + q_i y + r_i), i = 1,2 \quad (23)$$

where p_i,q_i and r_i are parameter sets.

Layer 5: This stage calculates the overall output as the sum of all input signals, each represented by a node in a circle shape and symbolized as Σ.

$$O_i^5 = \sum_{i=1}^{2} \overline{w_i} f_i = \frac{\sum_{i=1}^{2} w_i f_i}{\sum_{i=1}^{2} w_i} \quad (24)$$

In this context, w_i and f_i stand for the weight and input signal of the i-th input node, respectively. The output O_i^5 signifies the total of weighted input signals, adjusted by the sum of the weights.

Considering that ANFIS relies on gradient descent and the chain rule for learning, determining the error rate for each output node during training data is crucial. Assuming the output of the node at the ith position as O_i within a training dataset containing P entries, the error function can be evaluated as

$$E_p = \sum_{m=1}^{\#(L)} (T_{m,p} - O_{m,p}^L)^2 \quad (25)$$

The measure of error, calculated as the sum of squared errors, is represented by E_p. $T_{m,p}$ represents the mth component

of the target vector from output p, while $O_{m,p}^{L}$ represents the mth component of the actual output vector.

Therefore, the error rate can be calculated with the following equation

$$\frac{\partial E_p}{\partial O_{i,p}^{k}} = \sum_{m=1}^{\#(k+1)} \frac{\partial E_p}{\partial O_{m,p}^{k+1}} \frac{\partial O_{m,p}^{k+1}}{\partial O_{i,p}^{k}} \tag{26}$$

The error rate of an internal node has a range of values 1 ≤ k ≤ L − 1. Therefore, for all 1 ≤ k ≤ L and 1 ≤ i ≤ #(k), obtained equation (26). Now, we possess α as a parameter within the adaptive network.

$$\frac{\partial \mathrm{E}}{\partial \alpha} = \sum_{\mathrm{O}* \in \mathrm{S}} \frac{\partial E_p}{\partial O^*} \frac{\partial O^*}{\partial \alpha} \tag{27}$$

S represents the collection of nodes influenced by α. The derivative of the overall error measurement E concerning α is

$$\frac{\partial \mathrm{E}}{\partial \alpha} = \sum_{p=1}^{p} \frac{\partial E_p}{\partial \alpha} \tag{28}$$

Therefore, the update formula for the generic parameter α can be written as follows:

$$\Delta\alpha = -\eta \frac{\partial \mathrm{E}}{\partial \alpha} \tag{29}$$

where η = is a learning rate. The learning rate can be written as:

$$\eta = \frac{k}{\sqrt{\sum_{\alpha} (\frac{\partial \mathrm{E}}{\partial \alpha})^2}} \tag{30}$$

Here, k represents the size of each step length during the gradient transition in the parameter space. Hence, by employing Equations (20) and (23), we can formulate the propagation model for close-range wireless communication within forest, jungle, and open dirt road environments as follows;

$$\frac{\sum_{k=0}^{n} \frac{\mathbf{1}}{\mathbf{1} + (\frac{\boldsymbol{x} - \boldsymbol{c_i}}{\boldsymbol{a_i}})^{2*\boldsymbol{b_i}}} \frac{\mathbf{1}}{\mathbf{1} + [\,(\frac{\boldsymbol{x} - \boldsymbol{c_i}}{\boldsymbol{a_i}})^{2*\boldsymbol{b_i}}\,]} \boldsymbol{F_i}}{\sum_{k=0}^{n} \frac{\mathbf{1}}{[\,(\frac{\boldsymbol{x} - \boldsymbol{c_i}}{\boldsymbol{a_i}})^{2*\boldsymbol{b_i}}\,] \mathbf{1} + [\,(\frac{\boldsymbol{x} - \boldsymbol{c_i}}{\boldsymbol{a_i}})^{2*\boldsymbol{b_i}}\,]}} \tag{31}$$

Where x symbol represents input variables like frequency, bandwidth, spreading factor, range, and more, a defines the width of the input's membership function, while b shapes the curve on each side of the midpoint, c determines the center point of the membership function. F_i signifies the constant output level automatically generated by ANFIS.

3. Results and Discussion

3.1. Fuel Cell Test Results without Load

The initial testing phase for the open cathode PEM fuel cell was conducted under no-load conditions. This test was conducted both experimentally and through simulation. This experiment holds significance in elucidating the fuel cell output voltage behavior under no electrical load conditions. The stress data obtained from the experiment is subsequently utilized to validate the simulation model. An experiment was conducted for one hour to reach the maximum voltage without a load, achieved by providing a hydrogen flow input ranging from 1 to 10 L/min. The experimental results indicate that the minimum output voltage without a load is 74.425 volts, as depicted in Fig. 6.

Fig. 6. Results of minimum output voltage measurement without a load.

The hydrogen flow is gradually increased every 5 minutes until it reaches the maximum voltage stability value. Fig. 7 displays the measured maximum voltage of the unloaded fuel cell, recorded as 76.446 volts using a DC voltmeter.

Fig. 7. Results of maximum output voltage measurement without a load.

In Fig. 8, the response of the output voltage to the introduction of hydrogen gas is depicted. According to experimental results, it takes the fuel cell approximately 15 minutes to reach its maximum output voltage in the absence of a load.

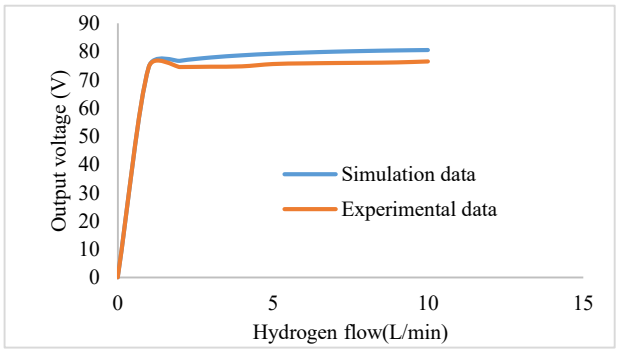

Fig. 8. Response of the fuel cell output voltage without load current.

3.2. Fuel Cell Test Results Under Various Load Current Conditions

In subsequent experiments, the fuel cell underwent a systematic loading process, varying from 1 A to 10 A, to comprehensively understand its behavior and performance characteristics, including how quickly it can adapt to changes in power demand. The fuel cell used in this research has a maximum power capacity of 2500 W. However, to assess the performance of the control system, it was tested under a power usage of 252.403 W.

Fig. 9. Experimental results for 1 A load current.

Experimental results obtained under a 1 A current load and a constant hydrogen flow of 8 L/min show that the fuel cell output power is 54.61 W, accompanied by a voltage of 54.634 V, as depicted in Fig. 9, Subsequently, based on the experimental and simulation results, a curve depicting the relationship between current and fuel cell voltage was generated, as illustrated in Fig. 10.

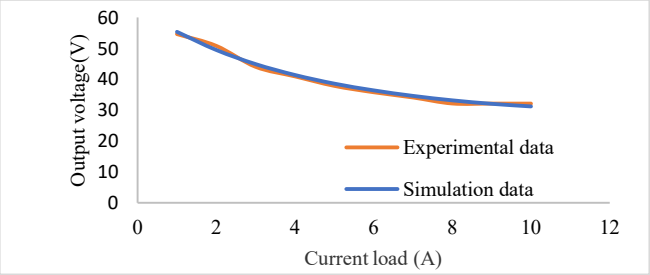

Fig. 10. The relationship curve between output voltage and current load.

The relative error (R) between simulation results (Vs) and experiments (Ve) can be calculated using Equation (29).

$$R = \frac{|V_s - V_e|}{V_e} \quad (32)$$

According to Equation (29), the calculated relative error for Fig. 11 is 1.8%, while for Fig.12 it is 1.9%. These results suggest that the fuel cell model is suitable for use.

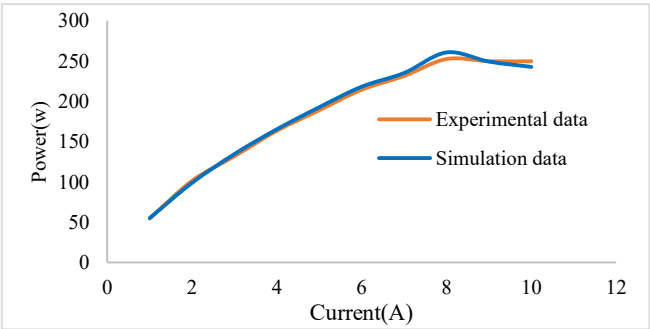

Fig.11. The relationship curve between power and current.

Fig. 10 and 11 present averaged measurement results for load current, voltage, and power, considering the fluctuations. Fig. 12 displays the experimental results obtained with a constant hydrogen gas input of 7.817 L/min. It's noticeable that the load fluctuates, leading to inaccuracies in the control system. Based on experimental findings, fluctuations are relatively minor within the range of 1 A to 7 A loads. However, beyond 7 A, these fluctuations become notably pronounced, as illustrated in Fig. 12. At a certain time, there is an increase in frequency and amplitude in the current load. Hence, the requirement for a control system capable of addressing this issue.

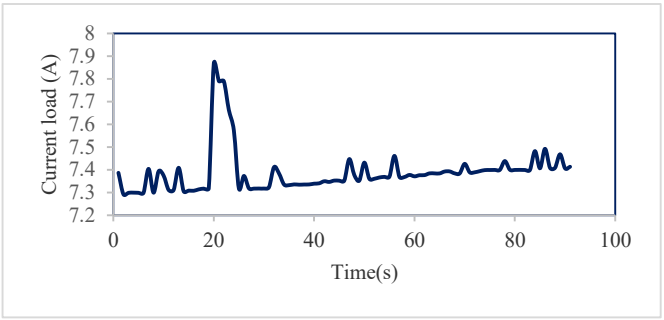

Fig. 12. Experimental results of load fluctuations with an 7.817 L/min hydrogen input.

3.3. Performance Test Results Of The Feedforward Wavelet Clipping-ANFIS Controller.

In this simulation, the current is employed both as a setpoint and feedforward parameter. Fig, 14 depicts the control system's response through the fuel cell current output. The control system demonstrates high stability and accuracy. The setpoint, aimed at 7.5 A, aligns closely with the output current response at 7.53 A. Based on the main performance index of the control system indicates an Integral Squared Error (ISE) of the control system stands at 0.09, with a settling time of 0.217 seconds and a rise time of 0.032 seconds within the closed-loop control system.

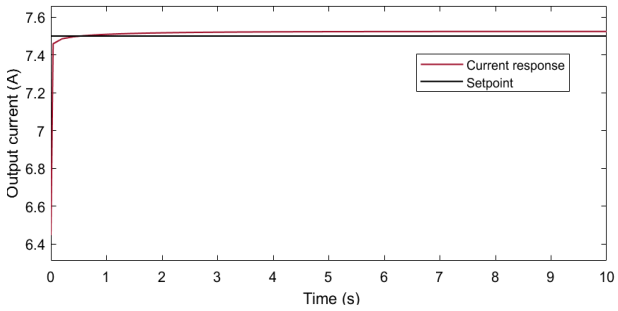

Fig. 13. Current output response.

Fig. 14 shows the hydrogen flow output response as the load transitions from 7.5A to 7.4A and then rises back to 7.6A. The control system showcases a rapid recovery, achieving a response time of 0.2 seconds.

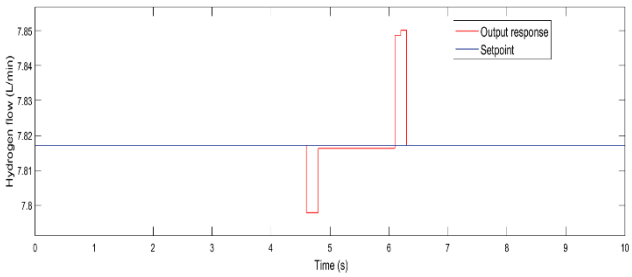

Fig. 14. Hydrogen flow output response.

4. Conclusion

This paper introduces a novel hybrid control method designed to regulate the hydrogen flow rate to the open cathode PEM fuel cell using feedforward wavelet clipping-

ANFIS. The primary objective of this control system is to enhance both the accuracy and speed of the system's dynamic response, particularly during disturbances arising from rapid load changes. The control mechanism functions to minimize fluctuations in the amplitude and frequency of the current output, ensuring that the hydrogen flow, controlled through current manipulation, maintains stability and precisely reaches the set point value. To evaluate the performance of the control system, integral square error (ISE), response time, and recovery time criteria are employed. The measured ISE criteria yield a value of 0.09, indicating heightened accuracy with a lower ISE value. Additionally, the settling time and rise time values of 0.217 seconds and 0.032 seconds, respectively, in the closed-loop control system illustrate a rapid dynamic response to load changes and a swift recovery time of 0.2 seconds in the face of disturbances.

In this study, our focus is solely on hydrogen flow control. In future research, we will explore the application of the MIMO technique to concurrently control the flow of both hydrogen and oxygen in an open cathode PEM fuel cell.

Acknowledgements

The authors would like to acknowledge Universitas Mercu Buana (UMB) Jakarta, Indonesia for the financial support. Thanks also to National Research and Innovation Agency of The Republic of Indonesia (BRIN) and Universiti Tun Hussein Onn Malaysia (UTHM) for their scientific and substantial support.

References

[1] B. Zafar, "Design of a Renewable hybrid photovoltaic-Electrolyze-PEM/Fuel Cell System using Hydrogen Gas," Int. J. Smart grid, vol. 3, no. 4, 2019, doi: 10.20508/ijsmartgrid.v3i4.83.g68.

[2] S. S. Kumar, M. Cirrincione, V. Léchappé, K. R. Ram and A. Mohammadi, "A simplified control oriented model of an open cathode PEM fuel cell," 2021 IEEE 12th Energy Conversion Congress & Exposition - Asia (ECCE-Asia), Singapore, Singapore, 2021, pp. 2415-2420,doi:10.1109/ECCE-Asia49820.2021.9479098.

[3] C. Mahjoubi, J. C. Olivier, Sondes S. Mustapha, M. Machmoum, I. S. Belkhodja, "An improved thermal control of open cathode proton exchange membrane fuel cell," Int. J. Hydrogen Energy, vol. 44, no. 22, pp. 11332–11345, 2018, doi: 10.1016/j.ijhydene.2018.11.055.

[4] F. Chen, L. Zhang, and J. Jiao, "Modelling of humidity dynamics for open-cathode proton exchange membrane fuel cell," World Electr. Veh. J., vol. 12, no. 3, 2021, doi: 10.3390/wevj12030106.

[5] Y. Song, C. Zhang, A. Deshpande, K. Tan, and M. Han, "Fixed air flow-rate selection by considering the self-regulating function of low power air-cooled PEMFC stack," Int. J. Heat Mass Transf., vol. 158, p. 119771, 2020, doi: 10.1016/j.ijheatmasstransfer.2020.119771.

[6] R. E. Rosli, E. H. Majlan, S. A. Abd. Hamid, W. R. W. Daud, R. Mohamed, T. Husaini, D. Rohendi, "Study of hydrogen consumption by control system ın proton exchange membrane fuel cell," Malaysian J. Anal. Sci., vol. 20, no. 4, pp. 901–912, 2016, doi: 10.17576/mjas-2016-2004-26.

[7] S. Gherairi, "Zero-emission hybrid electric system : estimated speed to prioritize energy demand for transport applications," Int. J. Smart Grid, vol. 3, no. 4, 2019..

[8] F. Migliardini, C. Capasso, and P. Corbo, "Optimization of hydrogen feeding procedure in PEM fuel cell systems for transportation," Int. J. Hydrogen Energy, vol. 39, no. 36, pp. 21746–21752, 2014, doi: 10.1016/j.ijhydene.2014.08.070.

[9] A. Thomya and Y. Khunatorn, "Design of control system of hydrogen and oxygen flow rate for proton exchange membrane fuel cell using fuzzy logic controller," in Energy Procedia, 2011, vol. 9, pp. 186–197. doi: 10.1016/j.egypro.2011.09.020.

[10] W. R. W. Daud, R. E. Rosli, E. H. Majlan, S. A. A. Hamid, R. Mohamed, and T. Husaini, "PEM fuel cell system control: A review," Renewable Energy, vol. 113. Elsevier Ltd, pp. 620–638, 2017. doi: 10.1016/j.renene.2017.06.027.

[11] M. Chandran, K. Palaniswamy, N. B. Karthik Babu, and O. Das, "A study of the influence of current ramp rate on the performance of polymer electrolyte membrane fuel cell," Sci. Rep., vol. 12, no. 1, pp. 1–10, 2022, doi: 10.1038/s41598-022-25037-0.

[12] S. Zhong, W. Yuan, X. Liu, J. Cao, and Y. Zhang, "Output power regulation system for portable micro fuel cell systems," Front. Energy Res., vol. 11, no. March, pp. 1–10, 2023, doi: 10.3389/fenrg.2023.1118743.

[13] E. S. Denisov, A. S. Salakhova, N. A. Adiutantov, and Y. K. Evdokimov, "Fluctuation-noise model for PEM fuel cell," IOP Conf. Ser. Mater. Sci. Eng., vol. 225, no. 1, 2017, doi: 10.1088/1757-899X/225/1/012110.

[14] J. Chilver-Stainer, A. F. A. Elbarghthi, C. Wen, and M. Tian, "Power output optimisation via arranging gas flow channels for low-temperature polymer electrolyte membrane fuel cell (PEMFC) for hydrogen-powered vehicles," Energies, vol. 16, no. 9, 2023, doi: 10.3390/en16093722.

[15] Y. Wang, X. Yang, Z. Sun, and Z. Chen, "A systematic review of system modeling and control strategy of proton exchange membrane fuel cell," Energy Rev., vol. 3, no. 1, p. 100054, 2024, doi: 10.1016/j.enrev.2023.100054.

[16] Y. Maiket, R. Yeetsorn, and W. Kaewmanee, "Hydrogen flow controller applied to driving behavior observation of hydrogen fuel cell performance test," ACS Omega, vol. 7, no. 43, pp. 38277–38288, 2022, doi: 10.1021/acsomega.2c02000.

[17] M. Fattahi, "Fuzzy sliding mode control of hydrogen flow in PEM fuel cell system for residential power generation," in 2017 5th International Conference on Control, Instrumentation, and Automation (ICCIA)

Fuzzy, 2017.

[18] F. C. Wang, L. H. Lin, and M. C. Chou, "Multivariable robust control for a 500W self-humidified PEMFC system," Eur. J. Control, vol. 17, no. 4, pp. 429–441, 2011, doi: 10.3166/ejc.17.429-441.

[19] S. and A. K. Darjat , Sulistyo, Aris Triwiyatno, "Designing hydrogen and oxygen flow rate control on a solid oxide fuel cell simulator using the fuzzy logic control method," Process, vol. 8, no. 154, pp. 1–22, 2020.

[20] L. Fan and Y. Liu, "Fuzzy logic based constant power control of a proton exchange membrane fuel cell," Prz. Elektrotechniczny, vol. 88, no. 5 B, pp. 72–75, 2012.

[21] Y. O. Tolga Özer, Tuba Nur Gul, "Hydrogen flow control by using fuzzy logic controller method for fuel cell power systems," in International Conference on Technics, Technologies and Education ICTTE 2014, 2014. [Online]. Available: https://sites.google.com/a/trakia-uni.bg/ictte-2014/

[22] Y. Qi, M. Thern, M. Espinoza-Andaluz, and M. Andersson, "Modeling and control strategies of proton exchange membrane fuel cells," in Energy Procedia, 2019, vol. 159, pp. 54–59. doi: 10.1016/j.egypro.2018.12.017.

[23] A. Abbaspour, A. Khalilnejad, and Z. Chen, "Robust adaptive neural network control for PEM fuel cell," Int. J. Hydrogen Energy, vol. 41, no. 44, pp. 20385–20395, Nov. 2016, doi: 10.1016/j.ijhydene.2016.09.075.

[24] Z. Cheng, P. Ren, Y. L. Xu, and H. N. Zhang, "Model and control of fuel supply systems of hydrogen/oxygen fuel cell," J. Eng., vol. 2017, no. 13, pp. 773–777, Jan. 2017, doi: 10.1049/joe.2017.0436.

[25] C. Y. Chuang, C. H. Lan, T. S. Lan, X. J. Dai, and J. H. Qin, "Flow control of proton exchange membrane fuel cell with theory of inventive problem solving (TRIZ)," Sensors Mater., vol. 33, no. 5, pp. 1603–1617, May 2021, doi: 10.18494/SAM.2021.3176.

[26] S. Divi, S. Das, G. Uday Bhaskar Babu, and S. H. Sonawane, "Fractional order PID controller design for supply manifold pressure control of proton exchange membrane fuel cell," Chem. Prod. Process Model., vol. 14, no. 3, Sep. 2019, doi: 10.1515/cppm-2018-0053.

[27] F. Behrooz, N. Mariun, M. H. Marhaban, M. A. M. Radzi, and A. R. Ramli, "Review of control techniques for HVAC systems-nonlinearity approaches based on fuzzy cognitive maps," Energies, vol. 11, no. 3, 2018, doi: 10.3390/en11030495.

[28] Y. Huang and Y. Huang, "Research on PID Parameter self-tuning speed control system based on grasshopper optimazation algorithm-optimized BP neural network," 2023 3rd Int. Conf. Energy, Power Electr. Eng., pp. 1444–1450, 2023, doi: 10.1109/epee59859.2023.10351813.

[29] S. Vadi, F. B. Gurbuz, S. Sagiroglu, and R. Bayindir, "Optimization of PI based buck-boost converter by particle swarm optimization algorithm," 9th Int. Conf. Smart Grid, icSmartGrid 2021, pp. 295–301, 2021, doi: 10.1109/icSmartGrid52357.2021.9551229.

[30] H. Housny, E. A. Chater, and H. El Fadil, "Fuzzy PID control tuning design using particle swarm optimization algorithm for a quadrotor," 2019 Int. Conf. Optim. Appl. ICOA 2019, pp. 1–6, 2019, doi: 10.1109/ICOA.2019.8727702.

[31] M. S. AbouOmar, H. J. Zhang, and Y. X. Su, "Fractional order fuzzy PID control of automotive PEM fuel cell air feed system using neural network optimization algorithm," Energies, vol. 12, no. 8, 2019, doi: 10.3390/en12081435.

[32] E. Bekiroglu and M. D. Yazar, "Improving fault ride through capability of DFIG with fuzzy logic controlled crowbar protection," 11th IEEE Int. Conf. Renew. Energy Res. Appl. ICRERA 2022, pp. 374–378, 2022, doi: 10.1109/ICRERA55966.2022.9922804.

[33] H. Beirami, A. Z. Shabestari, and M. M. Zerafat, "Optimal PID plus fuzzy controller design for a PEM fuel cell air feed system using the self-adaptive differential evolution algorithm," Int. J. Hydrogen Energy, vol. 40, no. 30, pp. 9422–9434, Aug. 2015, doi: 10.1016/j.ijhydene.2015.05.114.

[34] Q. Tian, "Theoretical ımplementations and optimization of construction machinery system based on fuzzy PID control considering limitations," Proc. - 4th Int. Conf. Smart Syst. Inven. Technol. ICSSIT 2022, pp. 676–679, 2022, doi: 10.1109/ICSSIT53264.2022.9716544.

[35] O. Erdinc, B. Vural, and M. Uzunoglu, "A wavelet-fuzzy logic based energy management strategy for a fuel cell/battery/ultra-capacitor hybrid vehicular power system," J. Power Sources, vol. 194, no. 1, pp. 369–380, 2009, doi: 10.1016/j.jpowsour.2009.04.072.

[36] N. Bizon, "Real-time optimization strategy for fuel cell hybrid power sources with load-following control of the fuel or air flow," Energy Convers. Manag., vol. 157, pp. 13–27, Feb. 2018, doi: 10.1016/j.enconman.2017.11.084.

[37] T. H. Kim, S. H. Kim, W. Kim, J. H. Lee and W. Choi, "Development of the novel control algorithm for the small proton exchange membrane fuel cell stack without external humidification," J. Power Sources, vol. 195, no. 18, pp. 6008–6015, 2010, doi: 10.1016/j.jpowsour.2009.12.009.

[38] H. Alzaq and B. Berk Ustundag, "A comparative analysis of multiplier-less 1-level discrete wavelet transform implementations on FPGAs," Proc. 2017 Int. Conf. Eng. Technol. ICET 2017, vol. 2018-Janua, no. August, pp. 1–6, 2017, doi: 10.1109/ICEngTechnol.2017.8308194.

[39] O. Hemakesavulu, M. P. Lalitha, P. B. Prasad, P. S. Babu, and M. Sowmiya, "Adaptive fractional order PID Based ANFIS for brushless DC motor speed control,"

12th IEEE Int. Conf. Renew. Energy Res. Appl. ICRERA 2023, pp. 295–299, 2023, doi: 10.1109/ICRERA59003.2023.10269384.

[40] J. S. Esmaeili, A. Akbari, A. Farnam, N. L. Azad, and G. Crevecoeur, "Adaptive neuro-fuzzy control of active vehicle suspension based on H2 and H∞ Synthesis," machines, vol. 11, no. 11, p. 1022, 2023, doi: 10.3390/machines11111022.

[41] Z. Abda, M. Chettih, and B. Zerouali, "Assessment of neuro-fuzzy approach based different wavelet families for daily flow rates forecasting," Model. Earth Syst. Environ., vol. 7, no. 3, pp. 1523–1538, 2021, doi: 10.1007/s40808-020-00855-1.

[42] E. H. M. Ndiaye, A. Ndiaye, and M. Faye, "Experimental validation of PSO and neuro-fuzzy soft-computing methods for power optimization of PV installations," 8th Int. Conf. Smart Grid, icSmartGrid 2020, pp. 189–197, 2020, doi: 10.1109/icSmartGrid49881.2020.9144790.

[43] Abdelnasir Omran, Alessandro Lucchesi, David Smith , Abed Alaswad, Amirpiran Amiri, Tabbi Wilberforce , Jos´e Ricardo Sodr´e , and A.G. Olabi., "Mathematical model of a proton-exchange membrane (PEM) fuel cell," Int. J. Thermofluids, vol. 11, p. 100110, 2021, doi: 10.1016/j.ijft.2021.100110.

[44] D. Ravi, S. S. Letha, P. Samuel, and B. M. Reddy, "An Overview of various DC-DC converter techniques used for fuel cell based applications," 2018 Int. Conf. Power Energy, Environ. Intell. Control. PEEIC 2018, pp. 16–21, 2018, doi: 10.1109/PEEIC.2018.8665465.

[45] K. Min, J. Brouwer, J. Auckland, F. Mueller, and S. Samuelsen, "Dynamic simulation of a stationary pem fuel cell system," ASME 2006 4th Int. Conf. Fuel Cell Sci. Eng. Technol. FUELCELL 2006, no. August, pp. 853–861, 2006, doi: 10.1115/FUELCELL2006-97039.

[46] G. Pourabedin and F. Ommi, "Modeling and performance evaluation of standalone solid oxide fuel cell for aircraft APU- II: Dynamic performance," Int. J. Smart grid, vol. 3, no. 1, 2019, doi: 10.20508/ijsmartgrid.v3i1.38.g44.

[47] J. Li and T. Yu, "Sensors integrated control of PEMFC gas supply system based on large-scale deep reinforcement learning," Sensors (Switzerland), vol. 21, no. 2, pp. 1–19, Jan. 2021, doi: 10.3390/s21020349.

[48] U. K. Chakraborty, "A new model for constant fuel utilization and constant fuel flow in fuel cells," Appl. Sci., vol. 9, no. 6, 2019, doi: 10.3390/app9061066.

[49] M. Li, M. Lin, L. Wang, Y. Wang, F. Pan, and X. Zhao, "Observation and analysis of ejector hysteresis phenomena in the hydrogen recirculation subsystem of PEMFCs," Entropy, vol. 25, no. 3, p. 426, 2023, doi: 10.3390/e25030426.

[50] S. Hegde and S. Ramachandran, "Implementation of Cdf 5 / 3 wavelet transform," no. 11, pp. 52–54, 2014.

[51] M. Gholipour, "Design and implementation of lifting based integer wavelet transform for image compression applications," Commun. Comput. Inf. Sci., vol. 166 CCIS, no. PART 1, pp. 161–172, 2011, doi: 10.1007/978-3-642-21984-9_14.

[52] B. Tang, K. Qin, and C. Chen, "A Novel clipping-based method to reduce peak-to-average power ratio of OFDM signals," pp. 1–11, 2020.

[53] B. Bakkas, R. Benkhouya, I. Chana, and H. Ben-azza, "Palm date leaf clipping : A new method to reduce PAPR in OFDM systems," 2020.

[54] G.P.N. Hakim, M.H. Habaebi, S.F. Toha, M.R. Islam, S.H.B. Yusoff, E.Y.T. Adesta, R. Anzum, "Near ground pathloss propagation model using adaptive communication in forest, jungle and open dirt," Sensors, vol. 22, no. 3267, 2022.